EXCITATION OF RADIAL P-MODES IN THE SUN AND STARS

ROBERT STEIN[1], DALI GEORGOBIANI[1], REGNER TRAMPEDACH[1],
HANS-GÜNTER LUDWIG[2] and ÅKE NORDLUND[3]

[1]*Michigan State University, East Lansing, MI 48824, U.S.A.; e-mail stein@pa.msu.edu*
[2]*Lund Observatory*
[3]*Astronomical Observatory, NBIfAFG*

Abstract. P-mode oscillations in the Sun and stars are excited stochastically by Reynolds stress and entropy fluctuations produced by convection in their outer envelopes. The excitation rate of radial oscillations of stars near the main sequence from K to F and a subgiant K IV star have been calculated from numerical simulations of their surface convection zones. P-mode excitation increases with increasing effective temperature (until envelope convection ceases in the F stars) and also increases with decreasing gravity. The frequency of the maximum excitation decreases with decreasing surface gravity.

1. Introduction

Acoustic (p-mode) oscillations have been observed in the Sun and several other stars (Deubner, 1975; Bedding and Kjeldsen, 2003). They are excited by entropy (non-adiabatic gas pressure) fluctuations and Reynolds stress (turbulent pressure) fluctuations produced by convection in the stellar envelopes. Expressions for the excitation rate have been derived by several people (Goldreich and Keeley, 1977; Balmforth, 1992; Goldreich, Murray, and Kumar, 1994; Nordlund and Stein, 2001; Samadi and Goupil, 2001). Evaluation of these expressions depends on knowing the properties of the convection. To obtain analytic results it is necessary to make drastic approximations to the convection properties. Unfortunately, both mixing length theory (Böhm-Vitense, 1958) and more recent theories of Canuto (Canuto and Mazzitelli, 1991) do not adequately describe the dynamics of convection and in addition contain free parameters and so lack predictive capability. Using results of numerical simulations of the near surface layers of a star it is possible to calculate the excitation rate of p-modes for the Sun and other stars without the need to make such approximations.

Here we describe the expression for the stochastic excitation of p-mode oscillations derived by Nordlund and Stein (2001) (Section 2) and the simulations used to derive the stellar convective properties (Section 3). We briefly present the properties of stellar envelope convection relevant to the excitation of oscillations (Section 4). Next the formula for p-mode excitation is applied to the Sun (Section 5). The results are in good agreement with observations. Excitation de-

creases at low frequencies because of increasing mode mass and decreasing mode compressibility. Excitation decreases at high frequencies because convection lacks high frequency motions. Finally, we apply our formula to the excitation of stellar p-mode oscillations using simulations of nine stars near the main sequence and a cool sub-giant (Section 6). We find that the total excitation over the entire star increases with increasing effective temperature and decreasing surface gravity.

2. Excitation Rate

The excitation rate can be derived by evaluating the PdV work of the non-adiabatic gas and turbulent pressure (entropy and Reynolds stress) fluctuations on the modes (Nordlund and Stein, 2001). This is a stochastic process, so the pressure fluctuations occur with random phases with respect to the oscillation modes. Therefore the excitation expression must be averaged over all possible relative phases. The resulting rate per unit area, with notation as in Nordlund and Stein (2001), is

$$\frac{\Delta\langle E_\omega\rangle}{\Delta t} = \frac{\omega^2 \left|\int_r dr \delta P_\omega^* \frac{\partial \xi_\omega}{\partial r}\right|^2}{8\Delta\nu E_\omega} \ . \tag{1}$$

This expression was targeted at analysis of data from numerical simulations, and operates with numerically well-defined quantities. A δ in front of a quantity, for example, denotes a so-called 'pseudo-Lagrangian' (not necessarily small) fluctuation relative to a fixed mass radial coordinate system (cf. Section 2, Nordlund and Stein, 2001, for further details).

The left-hand side of Equation (1) denotes the change of the kinetic energy of a mode with central frequency ω due to stochastic excitation, divided by the time interval Δt over which the change takes place. On the right-hand side, δP_ω^* is the discrete Fourier amplitude of the non-adiabatic, incoherent pressure fluctuations, as directly measured in a numerical simulation of duration $\Delta t = 1/\Delta\nu$. $\xi_\omega(r)$ is the mode structure of a radial p-mode at angular frequency ω, and $\partial\xi_\omega/\partial r$ is the mode compression. E_ω is the mode energy:

$$E_\omega = \frac{1}{2}\omega^2 \int_r dr \ \rho \ \xi_\omega^2 \left(\frac{r}{R}\right)^2 \ . \tag{2}$$

The appearance of E_ω in the denominator factors out the arbitrary normalization of $\xi_\omega(r)$. The mode eigenfunctions are evaluated from a complete envelope model, obtained by fitting the mean simulation radial structure to a deeper one-dimensional, adiabatic, convective envelope model.

The discrete Fourier transform is normalized such that the sum of squares of the absolute values of the discrete amplitudes equals the average of the squares of the fluctuations in time (Parseval's relation). As a consequence the magnitude of the discrete amplitudes P_ω^* that are measured in a simulation depend on the length

of the simulation, and Equation (1) contains a corresponding normalization factor $1/\Delta \nu = T$ (the length of the time interval).[1]

The pressure is the sum of turbulent pressure (Reynolds stress) and non-adiabatic gas pressure (entropy) fluctuations,

$$\delta P = \delta P_{\mathrm{turb}} + \delta P_{\mathrm{gas}}^{\mathrm{nad}} \; , \tag{3}$$

where the turbulent pressure fluctuation is

$$\delta P_{\mathrm{turb}} = \delta \langle \rho u_{\mathrm{r}}^2 \rangle_{\mathrm{horiz}} \; , \tag{4}$$

where u_r is the horizontally fluctuating radial velocity, relative to the pseudo-Lagrangian coordinate system. The non-adiabatic gas pressure fluctuation is

$$\delta P_{\mathrm{gas}}^{\mathrm{nad}} = P_{\mathrm{gas}} \left(\delta \ln P_{\mathrm{gas}} - \Gamma_1 \delta \ln \rho \right) \; . \tag{5}$$

The turbulent and non-adiabatic gas pressure fluctuations are calculated from the simulation at each 3D location at each saved time. The velocity, density and internal energy are obtained directly from the saved simulation data and the Γ_1 is found from the equation of state table. They are then averaged over horizontal planes and interpolated to the Lagrangian frame co-moving with the mean radial motion at each time. The fluctuations δP are the variations from their time average in the pseudo-Lagrangian coordinate system. The individual turbulence scales are not isolated, so the turbulent pressure and entropy fluctuations refer to the total convective contribution, including any interactions and phase relations among the different scales of motion.

Our expression for the mode excitation rate is similar to those derived by Balmforth (1992), Goldreich, Murray, and Kumar (1994) and Samadi and Goupil (2001). The excitation rate for all is proportional to the turbulent pressure and entropy induced pressure fluctuations times the gradient of the displacement eigenfunction divided by the mode mass. The main difference is that our expression contains the absolute value squared of the product of the pressure fluctuations with the mode compression, while the others contain the the absolute value squared of the mode compression times the sum of the absolute values squared of the turbulent pressure and entropy fluctuation contributions. Below we describe how this difference arises and its consequences.

Goldreich, Murray, and Kumar (1994) find that the increment in amplitude, A_ω, of a radial mode of frequency ω and radial eigenfunction ξ_ω during the lifetime $\tau_h \sim h/v_h$, of a single turbulent eddy of size h is (Goldreich, Murray and Kumar 1994, Equation (24))

$$\frac{\Delta A_\omega}{\tau_h} \sim \frac{i\omega}{\sqrt{2}} \Phi h^3 \left(\frac{\partial P}{\partial s} \delta s_h + \rho v_h^2 \right) \frac{\partial \xi_\omega^*}{\partial r} \; , \tag{6}$$

---

[1] If the power spectral density of the pressure is normalized per unit frequency interval, as is done by the other authors, then the total power is the time integral of the squared pressure amplitude rather than its average, and the factor $1/\Delta \nu$ disappears from the excitation expression (Equation (1)).

where v_h is the eddy velocity and δs_h its entropy fluctuation. Φ is the ratio of horizontal to vertical correlation lengths for the turbulence. The average excitation rate of the mode by a single eddy of size h is then taken to be

$$\frac{dE}{dt} \sim \frac{|\Delta A_\omega|^2}{\tau_h} \; . \tag{7}$$

By taking the square of the contribution from a single turbulent scale before integrating over the turbulence scales and depth it is implicitly assumed that there are no correlations between the turbulence at different scales and that the mode compression is constant over all turbulent eddies. This expression is then integrated over all eddies up to the maximum size for which $\omega\tau_h \leq 1$, to obtain (Goldreich, Murray, and Kumar, 1994, Equation 26, slightly rewritten)

$$\frac{dE_\omega}{dt} = \frac{\omega^2}{2} \int d^3r \left|\frac{d\xi}{dr}\right|^2 \int_0^{h_{\max}} dh\, h^2 \tau_h \left[\left(\rho u_{\mathrm{h}}^2\right)^2 + \left(\left(\frac{\partial P}{\partial s}\right)_\rho \delta s_{\mathrm{h}} \right)^2 \right] . \tag{8}$$

The eigenfunctions are normalized so that the mode energy is $E_\omega = 1/2 \langle |A|^2 \rangle \omega^2$ $M_\omega = \langle |A|^2 \rangle$, so there is no mode energy in the denominator.

Samadi and Goupil (2001) derived a comparable expression for the mode excitation. They make the explicit assumption that the mode compression, $\partial\xi/\partial r$, does not change on the length scale of the turbulence and so can be removed from the integral over the local turbulence. Further assuming that the turbulent excitation is isotropic, Samadi *et al.* (2003a, b) obtain for the excitation rate of radial modes

$$\begin{aligned}
\frac{dE_\omega}{dt} = \; & \frac{\pi^3 \omega^2}{4E_\omega} \int d^3r \frac{\Phi}{3} \rho^2 v^4 \left[\frac{16}{15} \frac{\Phi}{3} \left(\frac{d\xi_\omega}{dr}\right)^2 S_R + \right. \\
& \left. + \frac{4}{3} \frac{1}{\rho^2 v^2 \omega^2} \alpha_s^2 \delta s_{rms}^2 \left(\frac{1}{\alpha_s} \frac{d\alpha_s}{dr} \frac{d\xi_\omega}{dr} - i \frac{d^2\xi_\omega}{dr^2} \right)^2 S_S \right] ,
\end{aligned} \tag{9}$$

where $\alpha_s = (\partial P/\partial s)_\rho$ and S_R and S_S are Reynolds stress and entropy fluctuation contributions to the excitation.

Balmforth's (1992) results and assumptions are similar, but he restricts himself to considering only the Reynolds stress contributions in detail.

Our Equation (1) allows us to account for phase relations that are not accessible to other analyses. Consider, for example, the roles of the turbulent and non-adiabatic gas pressure contributions in Equation (1), and in the corresponding Equations (8–9). If, as is actually the case (cf., Stein and Nordlund, 2001), the turbulent and gas pressure fluctuations are correlated, and partially out of phase, then it is important that these two contributions are added linearly, as in Equation (1), rather than quadratically, as in Equations (8–9). Furthermore, with access to actual pressure fluctuations from numerical simulations, it is possible to correctly take into account correlations in the radial directions by performing the multiplication

of the mode compression factor $\partial \xi_\omega / \partial r$ inside the integral sign. If, for example, the pressure fluctuations generated by convection tend to be correlated over distances over which the factor $\partial \xi_\omega / \partial r$ changes sign, then in the detailed expression Equation (1) a partial cancellation occurs (correctly), which the analytically oriented expressions cannot include, due to the lack of information about correlations of the driving pressure fluctuations with depth.

Applying any of these expressions to calculate the mode excitation for a particular star requires knowledge of the properties of the convective turbulence for that star. Here as well, there are significant differences between simple analytic expressions for the spectra of the turbulent pressure and entropy fluctuations and those obtained from numerical simulations. Samadi *et al.* (2003a, b) investigate in detail the effects of different assumptions about the turbulence properties on the p-mode excitation rate. They find that the mode driving is particularly sensitive to the turbulence anisotropy factor and to the dynamic properties of the turbulence as represented by the temporal part of the turbulence spectrum. Using the simulation results, fit by analytic expressions for these factors, increases the excitation rate and the contribution of turbulent pressure relative to that of entropy fluctuations. The results from Equation (9) then approach the results using Equation (1).

3. The Simulations

We simulate a small portion of the photosphere and the upper layers of the convection zone by solving the equations of mass, momentum and energy conservation. Spatial derivatives are calculated using third order splines vertically and 5th order compact derivatives horizontally on a non-staggered grid. Time advance is a third order leapfrog scheme (Hyman, 1979; Nordlund and Stein, 1990). The calculation is stabilized by explicit diffusion in all the conservation equations using a hyperviscosity which enhances the diffusion on the scale of a few grid zones and decreases it for larger scale variations.

A significant, sometimes dominant, form of energy near the top of surface convection zones in stars is ionization energy. Hence, we use a tabular equation of state which includes LTE ionization and excitation of hydrogen and other abundant elements and the formation and ionization of H_2 molecules. This is necessary to obtain the correct relation between energy flux and fluid velocities and temperature fluctuations.

Radiative energy exchange is critical in determining the structure of the upper convection zone. Escaping radiation cools the plasma that reaches the surface, which produces the low entropy plasma whose buoyancy work drives the convection. Since the top of the convection zone occurs near the level where the continuum optical depth is one, neither the optically thin nor the diffusion approximations give reasonable results. We need to solve the 3D, LTE, non-gray radiation transfer in our models (Nordlund, 1982; Stein and Nordlund, 2003). To

obtain the radiative heating and cooling, the Feautrier equations are integrated along one vertical and 4 slanted rays (which are rotated each time step) through each grid point on the surface with the opacity and Planck functions interpolated to the intersection of the rays with each horizontal plane. The radiative transfer calculation is sped up by drastically reducing the number of wavelengths at which we solve the Feautrier equations, by using a multi-group method where the opacity at different wavelengths is collected into 4 bins according to its magnitude, with the Planck (source) function similarly binned. As a result, all wavelengths in a given bin have optical depth unity at approximately the same geometrical depth so that integrals over optical depth commute with the sum over wavelengths.

The boundaries of the computational domain are 'virtual boundaries'. The region we simulate is, in reality, coupled to an external medium, about which we have no information, and is influenced by what happens there. Given our lack of information on what is occurring outside our computational domain, the best that can be achieved are boundary conditions that are stable and introduce few artifacts. Horizontal boundaries are periodic – what goes out one side comes in the other. This allows the formation of granules and mesogranules, but removes the effect of supergranular flows on our calculation. Vertical boundaries are transmitting, with the entropy of the inflowing fluid at the bottom of the domain specified (which fixes the energy flux). Since ascending plasma below the superadiabatic layer is nearly isentropic and uniform and since convection is driven from the thin thermal boundary layer where energy transport switches between convective and radiative at the top of the convection zone which is included in our domain, the unknown influences from the external regions are small.

Simulations have been made of the Sun, 6 solar-like stars (Trampedach *et al.*, 1999), and F V, K V and K IV stars (Ludwig and Nordlund, 2000), all with solar composition. Since the simulation domains are shallow, only a few eigenmodes are present. To obtain all the eigenfunctions the deeper portions of the stellar envelopes must be included. For the solar-like stars the envelopes were extended inwards by matching the mean structure from the 3D simulations to 1D mixing length envelope models. The eigenfunctions of the other three stars were calculated from pure 1D mixing length models which match the entropy jump in the hydrodynamical simulations.

4. Convection Properties

Convection is driven by radiative cooling in the thin thermal boundary layer near the stellar surface. Only the fluid that reaches within a few photon mean free paths of the surface radiates away its energy and entropy. This low entropy fluid that has lost its energy near the surface is denser than its surroundings and is pulled back down into the interior by gravity. It forms the cores of downdrafts. These cool, low-entropy, filamentary, turbulent, downdrafts plunge many scale heights through
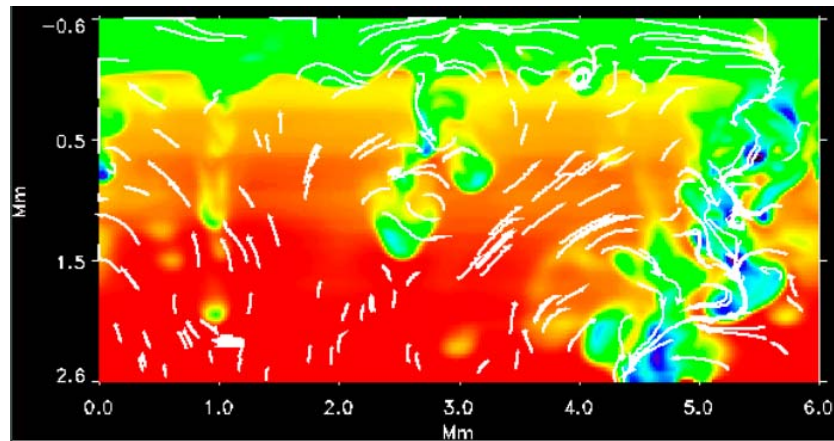
Figure 1. Temperature fluctuations and flow velocities on a vertical slice through the simulation domain. *Red* is hot and *blue* is cool. The fairly laminar upflows and turbulent downflows are clear.
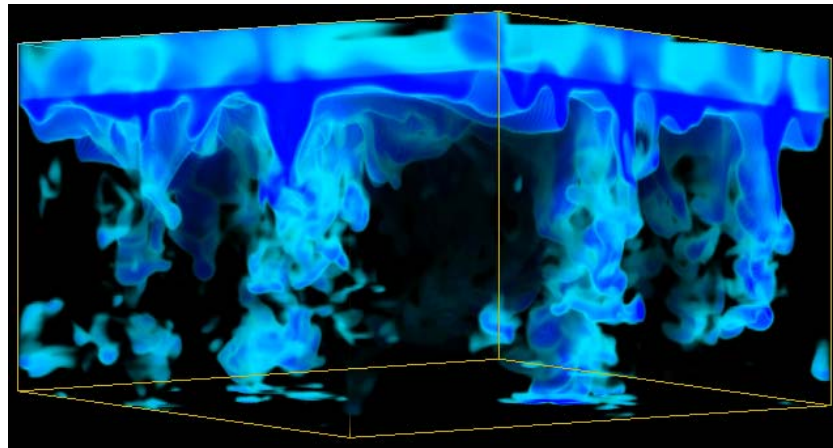

Figure 2. 3-D rendering of entropy. The downdrafts have large entropy fluctuations (*blue* and *green*) while the upflows have nearly uniform entropy.

warm, entropy-neutral, smooth, diverging, fairly laminar upflows (Figures 1–2 – see Stein and Nordlund, 1998, 2000, for more details.) The turbulent downdrafts have the largest turbulent pressure and entropy variations (Figure 3), and are the site of most of the excitation of the p-mode oscillations (Stein and Nordlund, 2001).

5. Excitation of Solar Oscillations

To obtain the total excitation rate *per mode* for the entire Sun we multiply the excitation rate per unit area (Equation (1)) by the area of the simulation (36 Mm^2). The reason for this seemingly paradoxical application of Equation (1) is the stochastic
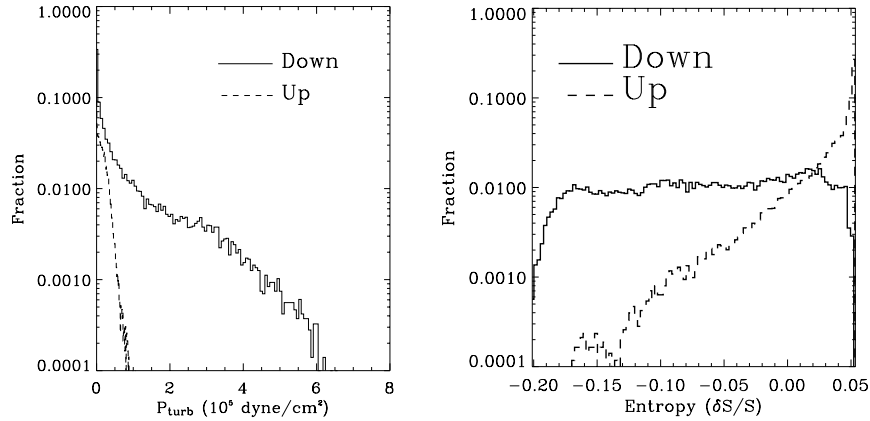
Figure 3. Turbulent pressure (*left*) and entropy (*right*) probability distribution functions separately for upflows and downflows near the surface. Both the turbulent pressure and the entropy fluctuations are much larger in the downdrafts which leads to most of the p-mode excitation occurring in the downdrafts.

nature of the fluctuations that occur in the models. Multiplying the expression with the total surface area of a star would clearly be incorrect, for example, since the periodic boundaries of the model would correspond to fluctuations that were perfectly correlated over the entire surface area. Consider instead the situation (which actually applies to a good approximation) where a doubling of the model size would correspond to simultaneously evolving four essentially uncorrelated areas of the original size. The pressure fluctuations δP_ω^* that enter into Equation (1) are the temporal fluctuations, after horizontal averaging. A four times larger area, containing four times as many uncorrelated random fluctuation, results (by random walk arguments) in a horizontal average with only half as large residual pressure fluctuations. After squaring and multiplication with the four times larger area, the same result is obtained. This demonstrates that the correct procedure for obtaining the global excitation rate per mode indeed is to multiply the excitation computed by using the measured, residual fluctuations from averaging over the extent of the model, with the area of the model, not the area of the star. The *total* stochastic excitation, on the other hand, grows in proportion to area (is constant per unit area), since the number of (non-radial) modes grows in proportion to area.

In practice, since our simulation domain is large enough to include a mesogranule, the pressure fluctuations in the frequency range relevant for p-mode excitation (due primarily to granules) are indeed nearly uncorrelated on scales larger than the model. There is a small correlated pressure fluctuation from supergranules, which is not modeled in the simulation, but the time scales are not relevant for p-mode excitation. To illustrate the point we measured the excitation power over areas of
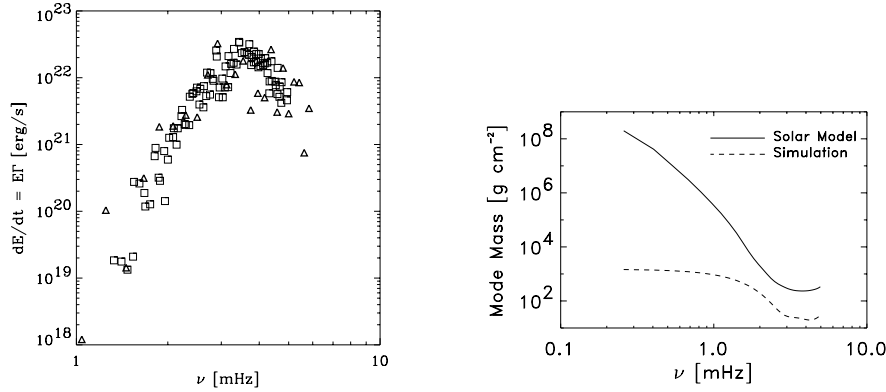
Figure 4. Comparison of observed and calculated p-mode excitation rates for the entire Sun left). *Squares* are from SOHO GOLF observations for $\ell = 0-3$ (Roca Cortes *et al.*, 1999) and *triangles* are the simulation calculations. Mode mass for solar and simulation modes (*right*). Mode mass increases at lower frequencies because the eigenfunctions extend deeper. The mass of the simulation modes becomes constant because the computational domain is limited in depth.

2×2 and 6×6 Mm^2 and found them to differ by nearly a factor of nine; the rms pressure fluctuations squared multiplied by area, on the other hand, differed only by about 3%.

The simulated solar excitation rates are in good agreement with the solar observations from SOHO (Figure 4). The excitation decreases at low frequencies because of the mode properties: the mode mass (or mode energy, E, in the denominator of Equation (1)) increases toward lower frequencies (Figure 4) and mode compression ($\partial \xi / \partial r$) (in the numerator of Equation (1)) decreases toward lower frequencies (Figure 5). The excitation decreases at high frequencies because of the convection properties: convection is a low-frequency phenomenon, so the turbulent pressure and non-adiabatic gas pressure (entropy) fluctuations (δP^* in Equation (1)) it produces decrease at high frequencies (Figure 5) (Stein and Nordlund, 2001).

P-mode excitation occurs preferentially close to the top of the convection zone, in the superadiabatic layer, where the turbulent velocities and the entropy fluctuations are largest (Figure 6). At low frequencies the overall driving is weaker, but it is spread fairly uniformly over a large depth. The peak driving is confined to within about 0.5 Mm of the surface. At high frequencies the driving becomes more and more concentrated close to the surface.
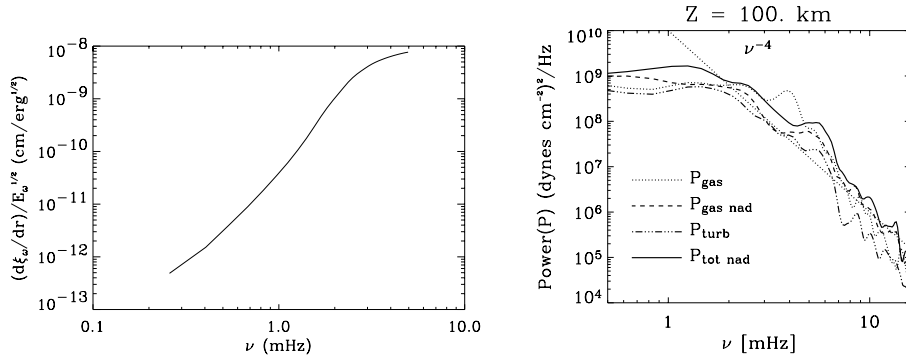
Figure 5. Mode compression at the surface (*left*) and pressure spectrum (*right*). The mode compression decreases toward low frequencies as the eigenfunctions vary more slowly. Their wavevector $k \approx \omega^2/g$. Both the turbulent and non-adiabatic gas pressure fluctuations decrease at high frequencies because the convective power decreases at high frequencies.
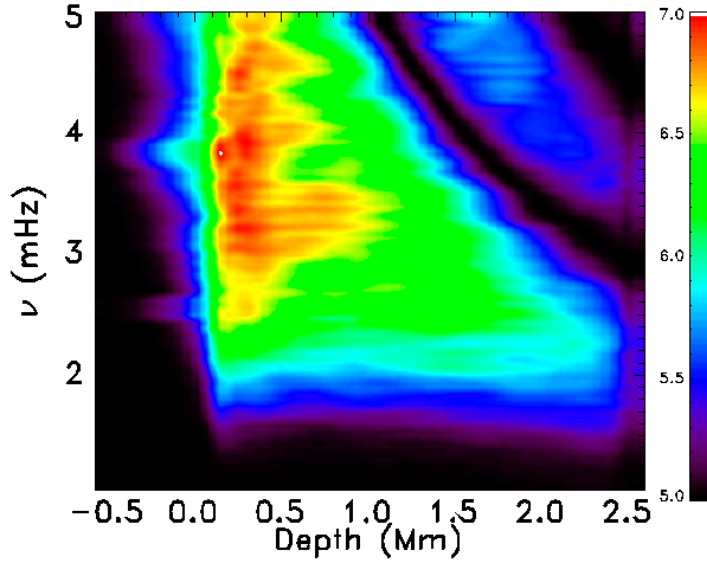

Figure 6. Logarithm (base 10) of the absolute value squared of the work integrand, normalized by the factors in front of the integral in Equation (1), $\omega^2 \left| \delta P_\omega^* \frac{\partial \xi_\omega}{\partial r} \right|^2 / 8 \Delta \nu E_\omega$ (in units of erg cm^{-4} s^{-1}) as a function of depth and frequency. Note that Equation (1) contains the square of an integral, which is influenced by phase factors that are difficult to visualize. To at least illustrate the overall depth and frequency dependence of the integrand the figure shows the absolute value squared of the integrand, modified by the frequency-dependent factors from Equation (1).
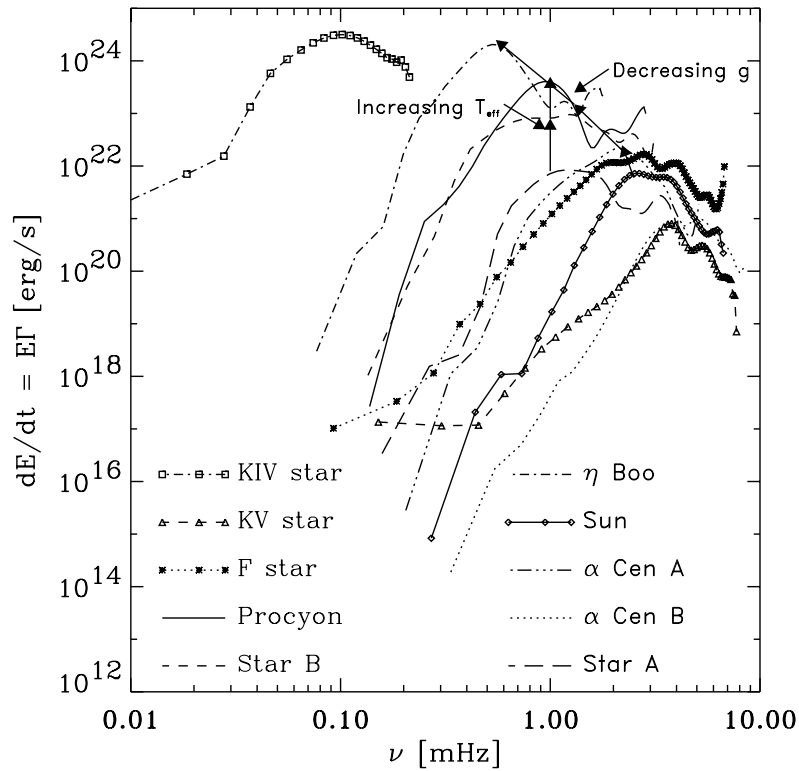
Figure 7. Excitation spectra of stars with different surface gravity and effective temperature. Maximum driving increases and occurs at lower frequencies for lower gravity. Driving increases with increasing effective temperature (until convection ceases for early F stars).

6. Stellar Excitation Rates

Simulations of convection in other stars have been used to calculate their p-mode excitation rates. As the surface gravity of the stars decreases, the maximum excitation rate increases and shifts to lower frequency (Figure 7). As the effective temperature of the stars increases (until surface convection ceases in the F stars) the excitation rate increases while the frequency of maximum driving remains unchanged (Figure 7). Maximum driving shifts to lower frequency with decreasing surface gravity because the buoyancy frequency and the acoustic cutoff frequency both decrease. The excitation rate increases with increasing effective temperature because a larger convective flux requires larger velocity and temperature fluctuations to transport more energy.

Turbulent pressure and non-adiabatic gas pressure contribute approximately equally (the turbulent pressure is slightly larger) to the mode excitation of most of the main sequence stars. For the hottest F star and for the subgiant K IV star
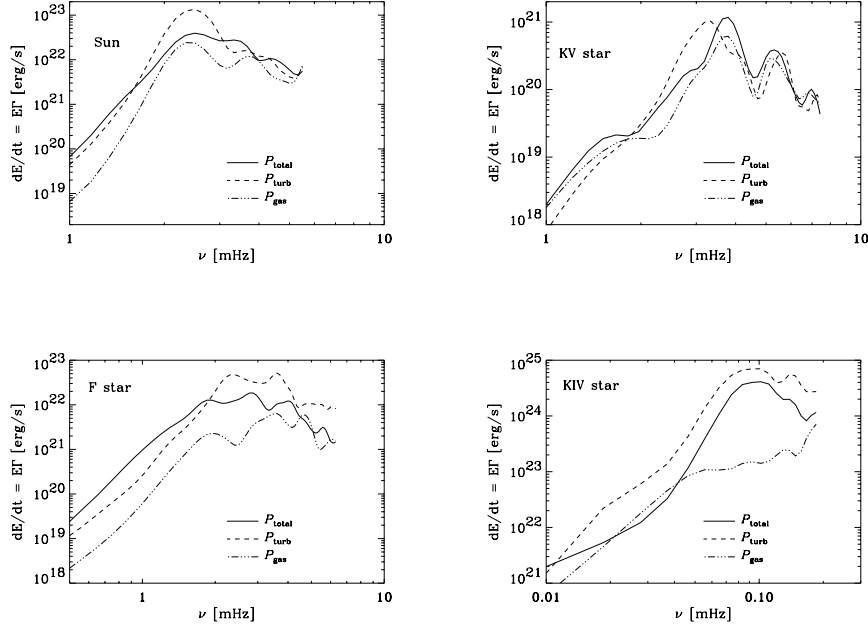
Figure 8. Total excitation and individual contributions from turbulent and non-adiabatic gas pressure fluctuations for the Sun, F, K V and K IV stars. For most main sequence stars the contributions from the two individual sources are nearly comparable, but for the hottest F star and the subgiant K IV star the turbulent pressure driving dominates.

the mode driving by turbulent pressure is significantly larger than the driving by the non-adiabatic gas pressure (Figure 8). Note that the total excitation is not equal to the sum of the individual turbulent and non-adiabatic gas pressure contributions. Sometimes there is destructive interference between them. The individual contributions of turbulent pressure and non-adiabatic gas pressure fluctuations to the frequency-integrated excitation for the entire stars as a function of effective temperature and surface gravity is shown in Figure 9.

The frequency-integrated total excitation rate for the entire star is shown as a function of effective temperature and surface gravity in Figure 10. The increase of driving with increasing effective temperature and decreasing surface gravity is clearly revealed.

7. Summary

P-modes are excited by the work of turbulent pressure (Reynolds stresses) and non-adiabatic gas pressure (entropy) fluctuations. The excitation decreases at low frequencies because of mode properties: the mode mass increases and the mode com-
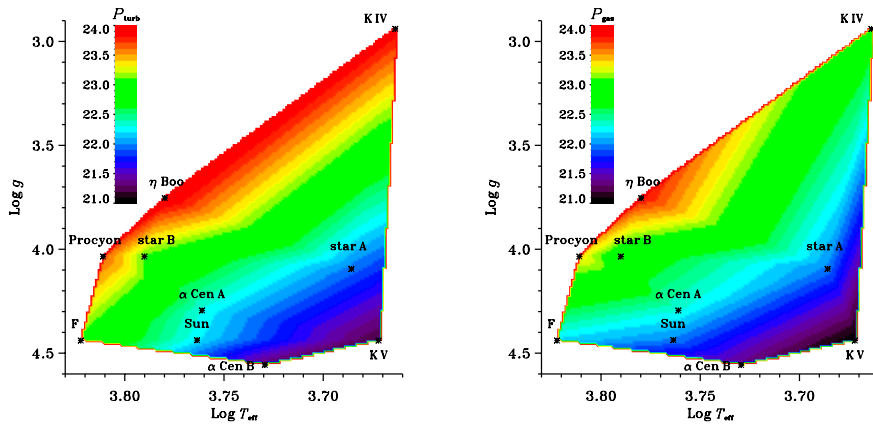
Figure 9. Individual contributions of turbulent (*left*) and non-adiabatic gas pressure (*right*) fluctuations to the frequency-integrated excitation for the entire star.
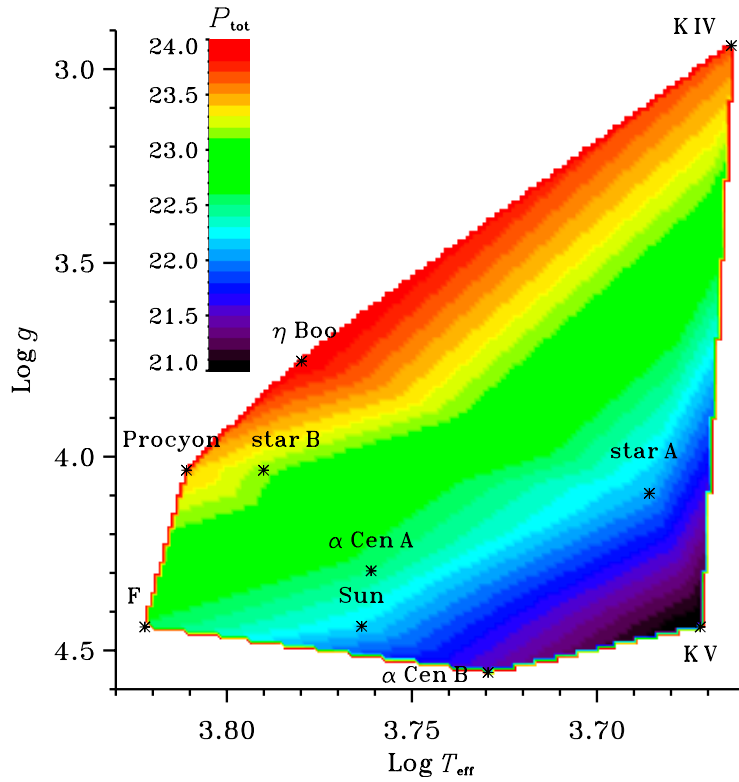

Figure 10. Frequency-integrated total excitation rate for the entire star increases with increasing effective temperature and decreasing surface gravity.

pression decreases toward lower frequencies. The excitation decreases toward high frequencies because of convection properties: convection has little high-frequency motions and so produces little high-frequency turbulent or non-adiabatic gas pressure fluctuations. The results of calculating the excitation of a few main sequence and one cool sub-giant star show that mode excitation increases with increasing effective temperature and decreasing surface gravity.

Acknowledgements

References

Balmforth, N. J.: 1992, *Monthly Notices Royal Astron. Soc.* **255**, 639.
Bedding, T. R. and Kjeldsen, H.: 2003, *Publ. Astron. Soc. Australia* **20**, 203.
Böhm-Vitense, E.: 1958, *Zeits. f. Astrophys.* **46**, 108.
Canuto, V. M. and Mazzitelli, I.: 1991, *Astrophys. J.* **370**, 295.
Deubner, F.-L.: 1975, *Astron. Astrophys.* **44**, 371.
Goldreich, P. and Keely, D. A.: 1977, *Astrophys. J.* **212**, 243.
Goldreich, P., Murray, N. and Kumar, P.: 1994, *Astrophys. J.* **424**, 466.
Hyman, J.: 1979, in R. Vichnevetsky and R. S. Stepleman (eds.) *Advances in Computer Methods for Partial Differential Equations III*, p. 313.
Ludwig, H.-G. and Nordlund, Å.: 2000, in L. S. Cheng, H. F. Chau, K. L. Chan, and K. C. Leung (eds.) *Proceedings of the Pacific Rim Conference, Hong Kong 1999*, Kluwer Academic Publishers, The Netherlands.
Nordlund, Å.: 1982, *Astron. Astrophys.* **107**, 1.
Nordlund, Å. and Stein, R. F.: 1991, in *Stellar Atmospheres: Beyond Classical Models*, D. Reidel, Dordrecht, p. 263.
Nordlund, Å. and Stein, R. F.: 2001, *Astrophys. J.* **546**, 576.
Roca Cortes, T., Montanes, P., Palle, P. L., Perez Hernandez, F., Jimenez, A., Regula, C., and the GOLF Team: 1999, in A. Gimenez, E. Guinan, B. Montesinos (eds.), *Theory and Tests of Convective Energy Transport, ASP Conf. Ser.* **173**, 305.
Samadi, R. and Goupil, M.-J.: 2001, *Astron. Astrophys.* **370**, 136.
Samadi, R., Goupil, M.-J., and Lebreton, Y.: 2001, *Astron. Astrophys.* **370**, 147.
Samadi, R., Nordlund, Å., Stein, R. F., Goupil, M.-J., and Roxburgh, I.: 2003a, *Astron. Astrophys.* **403**, 303.
Samadi, R., Nordlund, Å., Stein, R. F., Goupil, M.-J., and Roxburgh, I.: 2003b, *Astron. Astrophys.* **404**, 1129.
Stein, R. F. and Nordlund, Å.: 1998, *Astrophys. J.* **499**, 914.
Stein, R. F. and Nordlund, Å.: 2000, *Solar Phys.* **192**, 91.
Stein, R. F. and Nordlund, Å.: 2001, *Astrophys. J.* **546**, 585.
Stein, R. F. and Nordlund, Å.: 2003, in I. Hubeny, D. Mihalas and K. Werner (eds.), *Stellar Atmosphere Modeling, ASP Conf. Proc.* **288**, 519.
Trampedach, R., Stein, R. F., Christensen-Dalsgaard, J., and Nordlund, Å.: 1999, in A. Gimeénez, E. F. Guinan, and B. Montesinos (eds.), *Stellar Structure: Theory and Tests of Convection Energy Transport, ASP Conf. Series* **173**, 233.